

# On the Decomposition of Cell Clusters

Oliver Schmitt · Stephan Reetz

Published online: 13 August 2008  
© Springer Science+Business Media, LLC 2008

**Abstract** Successful segmentation of a multilevel to a bilevel microscopic cell image rather frequently gives rise to touching objects which need to be separated in order to perform object specific measurements. The standard approach of dealing with this problem is a watershed decomposition of gradient, distance or low pass filtered transforms. However, if cell clustering is excessive, the cell size varies and cells have various shapes that are different from circles the watershed approaches produce unsatisfying results.

We found a technique that splits cell clumps into meaningful parts. Since this method is based on the analysis of contour curvature on the scale space of Fourier coefficients relevant dominant points can be recognized. Based on an optimized heuristic approach pairs of these dominant points are recursively matched since splitted objects do not possess concavities respectively intrusions anymore. The advantages of this approach are (i) the independence of cell shapes which are clumped, (ii) the consideration of holes or background intensities within objects, (iii) the robustness in terms of convergence and a few parameters only to adapt to other families of decomposition problems.

The objective of this contribution is to explain the algorithm, show its results using different examples from benchmark databases, self generated images and complex configurations of cell images.

**Keywords** Segmentation · Decomposition · Subdivision · Perceptual grouping · Visual grouping · Splitting · Partitioning · Clump splitting · Aggregates · Touching particles · Partial occlusion · Overlapping objects · Fused objects · Aggregate particles · Juxtaposed objects · Cell cluster · Polygonal approximation · Curvature · Shape · Dominant points · Convexity · Concavity · Indentation · Protrusion · Fourier coefficients

## 1 Introduction

In dependence of the quality of staining of cells in histological sections [95] global segmentation performed by standard methods [46, 80, 93, 110, 120, 127] produce bilevel images that contain sufficient foreground information for further cell-object specific processing (Fig. 1b, c). Microscopic images of histological sections [78] always contain overlaps of structures because they are distributed in a relative thin section space that have in most cases a height of 3–60  $\mu\text{m}$  which is projected on the 2D-plane of an imaging sensor (Fig. 1a). Juxtapositioned objects appear clumped because their projections overlap partially or totally (Fig. 1b). These overlaps are reduced in confocal laser scanning microscopy (CLSM) [2, 5]. However, for long term measurements of large areas of histological sections, for instance serial sections of brains, CLSM is inapplicable and motorized video microscopy [97] or high resolution transparent flat bed scanning [96] need to be performed.

### 1.1 Decomposition of Cell Clusters

Cytological as well as histological analysis of cell parameters [21, 36, 65, 84, 87, 126] assume that the objects, i.e. cell bodies and/or cell nuclei, to be measured are not connected

---

O. Schmitt (✉)  
Institute of Anatomy, University of Rostock, 18051 Rostock,  
Germany  
e-mail: [schmitt@med.uni-rostock.de](mailto:schmitt@med.uni-rostock.de)

S. Reetz  
Institute of Mathematics, University of Rostock, 18051 Rostock,  
Germany  
e-mail: [stephan.reetz@uni-rostock.de](mailto:stephan.reetz@uni-rostock.de)

(Fig. 1c, d). Naive methods like conditioned and scale space based erosion [17] result in an unsatisfying splitting if objects are juxtaposed very closely. Even, sophisticated procedures like watershed segmentation of heavily clustered cells with different shape and size may fail [4, 11, 20, 24, 29, 57, 66, 76, 116–118].

Since many years [44, 45, 81, 82, 91, 101, 109, 112, 125] much effort has been spent to decompose such overlaps of cells because successful and robust splitting is the key for automation [68]. In cognitive psychology it has been suggested by Attneave [7] that information along visual contours is concentrated in regions of high magnitude of curvature, rather than being distributed uniformly along the contour. Attneave [7] indicates that most shape information is contained in the corners (high curvature points), which are able to characterize the contour. Recently, this has been investigated more precisely by Feldman and Singh [33] in regard to information theory [86, 103]. Furthermore, this is a broad area of research in cognitive science especially Gestalt psychology and perceptive psychology where components of objects are analyzed [9, 12, 33, 48, 64, 77, 106]. Gestalt theory has shown (based on the Gestalt principles of human perception: proximity, similarity, continuity, closure) that splitting may take advantage of the fact that two sharp inflections must be aligned before clusters are split [113]. Based on these perceptive principles synthetic images exhibiting object agglomerations can be splitted by an investigator to be used for comparison with partitions performed by an algorithm.

## 1.2 Overview of the Techniques for Splitting Fused Objects in Digital Images

Overviews of contemporary theories of visual form have been published by different authors [19, 67, 83, 128]. Another point of view of partitioning overlapping objects which are consequently connected in a projective image is the completion of each object contours in such a way that for each object its original boundary is determined [32, 114].

However, complex overlaps of hundreds or thousands of structures in images where the area of the foreground, i.e. cells, is larger than the background the decomposition problem becomes complex. Automatic morphometry [8] of complex cell distributions in histological sections of biologic material becomes a challenging task in combination with registration of serial sections [72] because complete cell atlases of organs especially brains can be generated. Especially in the mouse brain this approach is expected to become a cutting edge technology because mice are the most often used species for genetic modifications like knocking out or knocking in specific genes inducing different kinds of effects like morphological changes. These morphological effects must be recognized, analyzed and compared quantitatively at the cellular level.

Edge filtering in gray scale images (Sobel-, Roberts-, Prewitt-, Laplace of Gaussian-, zero-crossing-filter) could be a starting point to perform splitting in images offering relative strong contrasts of fore- and background. However, this is not the case in histological images of the central nervous system.

The Hough transform is a related method that carries out simple shape recognitions, too. These transforms are useful if particles possess regular shapes (circles or ellipses) [54]. However, morphology based separation can be adapted to different shapes of aggregated particles as shown by Talbot and Appleton [111]. Aggregates that consists of particles of certain sizes can be segmented by morphological approaches. The shape and size of cells in biological specimens may vary considerably: they may appear as two touching cells or large clusters with many holes, i.e. connected regions of background within an aggregate (Fig. 1b). For such complex clusters contour based algorithms are used. Mostly, these algorithms determine centroids of decomposed particles which are used thereafter for a precise gray scale based segmentation by the watershed method or region growing. Contour based algorithms determines dominant points, i.e. concavities and convexities of the contour and test which cut path or split path of opposite dominant points turns out to minimize a cost function.

Performing a skeletonization [14, 30] or thinning of the background may be useful because the derived endpoints of the medial axis are related to concavities of the foreground, i.e. the cell aggregate. These endpoints can be used by an appropriate chain of morphology techniques to obtain a partition. However, different medial axis transforms of complex cell aggregates may generate diverse skeleton networks requiring further intricate analysis.

Further methods aim to separate cells by applying active contours and level sets. A comprehensive overview of the literature concerning these families of aggregate-particle-problems and algorithms is given in the following:

- *Morphology based procedures* [6, 10, 24, 27, 53, 57, 59, 60, 71, 75, 76, 118, 122],
- *Contour based techniques* [1, 3, 13, 22, 23, 34, 35, 39, 47, 49, 50, 55, 56, 70, 89, 92, 94, 102, 111, 115, 119, 121, 124, 125],
- *Active contour based methods* [8, 18, 90, 100],
- *Graph theoretic approaches/topological maps* [15, 41, 42],
- *Parametric fitting algorithms* [26, 111, 121, 123] and
- *Level set approaches* [26, 98].

## 1.3 Decomposition by Means of Polygonal Approximation

The method of Wang [119] was developed originally to perform splitting of touching objects in images generated from projections of small pieces of rocks on a moving conveyor

belt. The silhouette boundaries of these binarized images have much in common with contours of aggregates of nerve cells. Therefore, we implemented this contour based technique. Because the small rocks analyzed by this method have rough contours Wang [119] simplifies the contour information by using polygonal approximation. Such a simplification has the advantage to keep the number of relevant coordinates of the contour small in order to reduce computation time. Furthermore, a distinction between types of corners [31, 104] is not necessary after polygonal approximation because graduations of the smoothness of corners can be reduced in dependence of the grid size. However, this technique depends strongly on the size of the grid assuming that most parts of the aggregates possess a similar size and contour characteristics. If image size, object sizes within the image or image resolution changes the grid size of the polygonal approximation must be adjusted. Beside this parameters of sizes the grid size depends on the contour characteristics, which have to be adjusted by parameters like compactness, shape factors and fractal dimension of the contour. Cell aggregates in the nervous system or other organs may consist of varying sizes of their constituting parts and have other contour characteristics. Because the decomposition of aggregates as proposed by Wang [119] strongly depends on the result of polygonal approximation we found an adaptive way to filter small concavities and convexities that are not needed for decomposition at the cellular level using a scale space approach [16, 73, 74].

Furthermore, contour based decomposition techniques seem to overcome disadvantages of iterative morphological techniques like splitting aggregates by the watershed algorithm [60, 118]. If aggregates are composed of particles with strong size variations, overlaps intermingled with background intensities contour information can be evaluated to obtain information for decomposition. Sometimes the density of cells varies strongly, however, microscopic illumination conditions stay constant resulting in an insufficient illumination with optically fused cells. If the preprocessing of these images is based on low pass filtered original gray values and not on a distance transform the watershed result will produce strong undersegmentations.

#### 1.4 Aims

The objective of this contribution is the presentation of a new decomposition method that is motivated by the technique of polygonal approximation published by Wang [119] that belongs to the class of contour based approaches. Since we observed some disadvantage of directly applying the original method of Wang [119] a new algorithm was worked out that differs principally from other techniques. Firstly, the curvature scale space decomposition (CSD) can be applied to images covering object aggregates of different topologies like multiple connected domains or holes. Secondly,

the problem of dominant concavities that are relevant for partitioning is approached by considering concavities in a *concavity scale space* build by presentations of Fourier coefficients of the boundary of the clusters. This new method leads to reliable partitioning results that need less parameters in comparison to the technique of Wang [119]. In order to present its advantages with regard to a larger class of partitioning problems different types of test images and real biological images were used.

The specific aim of this study is to decompose cell agglomerates in order to localize the cell borders (Fig. 1c, d). Based on the localization of cell borders in the form of closed polygons (Fig. 1c, d) the regions can be masked and intensity distributions of localized cells can be analyzed with pattern recognition techniques. The result of the partitioning of systematic modified test images and real biological images was compared with images in which an expected partition was defined by an investigator to allow comparisons of the splitting outcomes. At least we present a technique which optimizes internal parameters and gives rise to an almost robust decomposition method.

## 2 Material and Methods

### 2.1 Types of Images

For the development and testing of algorithms we used 3 families of images: synthetic images (*arte*) which are derived partly from IPAN test images ([http://visual.ipan.szaki.hu/corner/corner\\_click.html](http://visual.ipan.szaki.hu/corner/corner_click.html)) or Liu and Srinath [62] and Liu and Sclaroff [63], light microscopic images of cell clusters (*cells*) [97] and high resolution transparent flat bed scanned images [96] of histological sections of mouse brains stained with the modified method of Gallyas (*scan*) [38, 97].

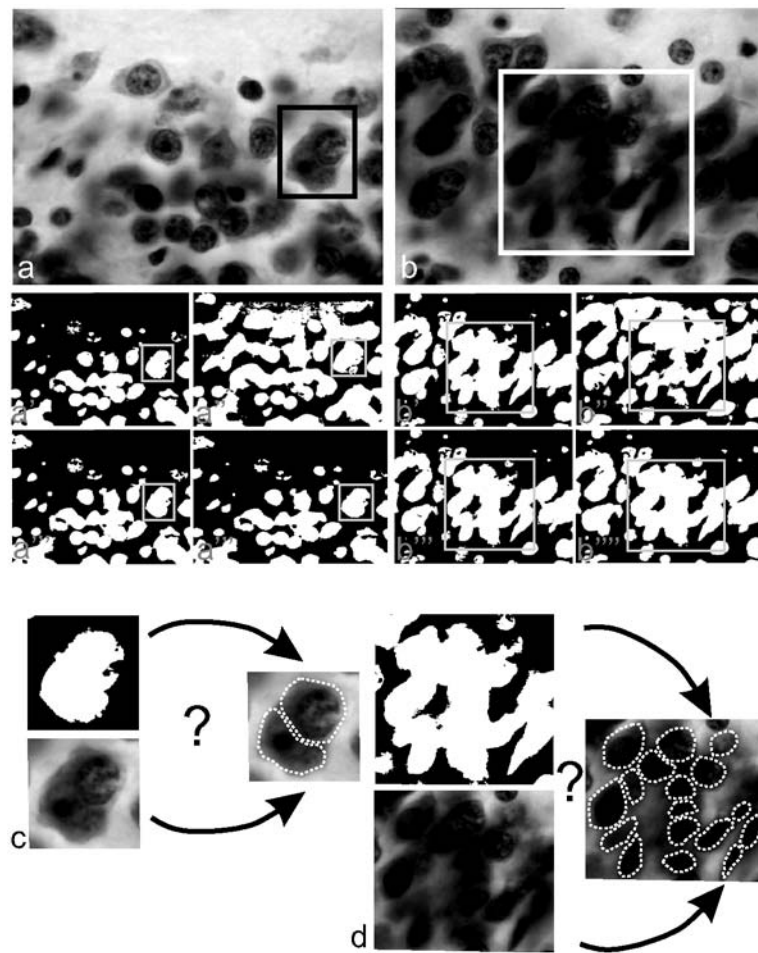
### 2.2 Definition of Images

An image can be modeled as a function defined on a rectangle  $Q = [a_1, b_1] \times [a_2, b_2] \subset \mathbb{R}^2$ . A gray level image has values in the interval  $[0, 255]$  where 0 means black and 255 is white. A binary image is a function with only two values 0 (black) and 1 (white). By sampling of an image, one obtains a digital image which can be represented as a matrix  $(b_{i,j})_{i,j=1}^{m,n}$ , with the gray-levels  $b_{i,j} \in \{0, 1, \dots, 255\}$ . A binary digital image  $(b_{i,j})_{i,j=1}^{m,n}$  is a matrix with binary entries  $b_{i,j} \in \{0, 1\}$ . In this paper, we will consider mostly binary images.

### 2.3 Expected Decomposition (ESD)

The expected decompositions are considered as the ground truth. They have been generated by experts in neurohistology to obtain a set of splittings for comparison with the algorithm results. These splittings are made on principles of

**Fig. 1** Illustration of the decomposition problem. (a) First sample image with a superposition of two disjoint nerve cells (*rectangle*). (b) Second sample image with a strong spatial clustering of cells (*rectangle*). (a') Global segmentation with the Otsu-method. (a'') Local adaptive segmentation. (a''') K-means segmentation. (a''') Mean-Shift segmentation (same as in b'-b'''). Binarizations are comparable: the segmentation results lead to strongly fused cell objects. (c) Superimposed gray scaled and binarized cells for which a decomposition should be found. At least the cell boundary should be reconstructed used for masking and further operations. (d) Clustered gray scaled and binarized cells for which a decomposition should be found and cell boundaries should be reconstructed



Gestalt theory. Due to these principles [9, 12, 33, 48, 64, 77, 106] components of objects are analyzed by investigators. Information along visual contours that is relevant for cognitive subdividing of objects is concentrated in regions of high magnitude of curvature [7], rather than being distributed uniformly along the contour. Attneave [7] indicates that most shape information is contained in the corners (high curvature points), which allows to characterize the contour. This has been investigated more precisely by Feldman and Singh [33] in regard to information theory [86, 103]. Based on the Gestalt principles *proximity*, *similarity*, *continuity*, *closure* of human perception experts were instructed to concentrate on sharp inflections possessing a topological relation in order to outline the split paths [113].

#### 2.4 Segmentation of Gray Scale Images and Object Boundaries

Gray level images were segmented by the global segmentation method of Otsu [79] followed by an opening and closing done with a symmetric structure element to remove oversegmented small regions resp., fill undersegmented small holes. As shown in Fig. 1 different segmentation approaches lead

to comparable results. In video microscopic images shading can be found due to inhomogeneous illumination. This need to be filtered by a suitable shading correction procedure or a local adaptive segmentation should be performed. In a binary image we consider all subsets with value 1. We assume that there exists finitely many subsets with value 1 which are (open and connected)  $C^2$ -domains. Let  $D \subset Q$  be such a simple connected  $C^2$ -domain. Then the boundary of  $D$  is a  $C^2$ -curve, which can be approximated by a closed polygon.

The coordinates of the contours of connected regions, resp., objects in binary images were determined and administered in a *cell* data type of Matlab (Mathworks). These boundaries or contours are considered in the following in more detail because the *curvature* of a discrete contour will be used later on.

#### 2.5 Watershed Based Decomposition

Watershed algorithms [69, 88] are a matter of common knowledge. Therefore, the watershed segmentation is not explained algorithmically. We applied the watershed decomposition (WSD) to compare with the approaches developed

here. Since there exist four basic preprocessing possibilities:

- 1) directly smoothing the gray level image,
- 2) distance transformations (chessboard, cityblock, euclidean, quasi euclidean) of a binary segmented image,
- 3) marker based WSD,
- 4) internal and external regions approach

for applying WSD (8-connected neighborhood) the euclidean distance transformation of binary segmented images was used here. Finally, the distance transformed images were smoothed by a  $5 \times 5$  median filter. In the last section, the WSD results will be presented first followed by the results of the new techniques.

## 2.6 Geometric Approach

### 2.6.1 Definitions of Polygon, Boundary Curve, Curvature and Compactness

A closed polygon with the vertices  $P_k \in Q$  ( $k = 0, \dots, n - 1$ ) is the union of line segments

$$\overline{P_0P_1} \cup \overline{P_1P_2} \cup \dots \cup \overline{P_{n-1}P_0},$$

which forms a positive oriented, simple closed curve (without double points). The interior of the closed polygon is a polygonal domain that approximate a single connected  $C^2$ -domain  $D$ . The closed polygon is oriented so that by circumscribing in positive orientation the interior lies at the left-hand side. The arc length of the closed polygon is equal to

$$\sum_{k=0}^{n-1} |P_k - P_{k+1}| \quad (P_n := P_0)$$

A closed  $C^2$ -curve  $X : I \rightarrow Q$  with the parameter presentation  $X(t) = (x(t), y(t))$  with ( $t \in I$ ) fulfills the following conditions:  $x \in C^2(I)$ ,  $y \in C^2(I)$  with  $x^{(k)}(a) = x^{(k)}(b)$ ,  $y^{(k)}(a) = y^{(k)}(b)$  ( $k = 0, 1, 2$ ) and  $(x'(t))^2 + (y'(t))^2 > 0 \forall t \in I = [a, b]$ .

If  $X$  is the boundary curve of a single connected  $C^2$ -domain  $D$ , then this curve is simple closed without double points. The arc length of the restricted curve  $X|[a, t]$  ( $t \in [a, b]$ ) is given by

$$s(t) = \int_a^t ((x'(u))^2 + (y'(u))^2)^{1/2} du \tag{1}$$

such that  $s(b) = P$  is the perimeter of  $D$ . The area of  $D$  can be computed by

$$A = \frac{1}{2} \int_a^b (-y(t)x'(t) + x(t)y'(t))dt. \tag{2}$$

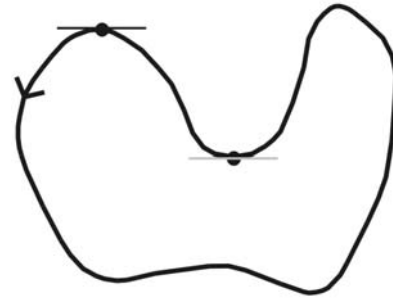


**Fig. 2** The arrow indicates the positive orientation of the curve. The black tangent passes a convexity with  $\chi(t) > 0$  and the gray tangent passes a concavity with  $\chi(t) \leq 0$

We consider only simple closed polygons, i.e. closed polygons without double points. Passing the polygon in the mathematical positive direction (anticlockwise, Fig. 2), the interior lies always on the left side. A vertex  $P_i$  is called *convex*, if the interior angle between  $\overrightarrow{P_iP_{i-1}}$  and  $\overrightarrow{P_iP_{i+1}}$  lies in  $[0, \pi]$ . Here, we set  $P_{-1} := P_{n-1}$ . In the other case the vertex is *concave*.

The **curvature**  $\chi$  of the curve  $X$  at  $t \in I_1$  can be calculated by

$$\chi(t) = \frac{x'(t)y''(t) - x''(t)y'(t)}{[(x'(t))^2 + (y'(t))^2]^{3/2}}. \tag{3}$$

Passing the curve in the anticlockwise direction then curvatures are positive for convexities and nonpositive for concavities ( $\chi \leq 0$ )

If a connected region with perimeter  $P$  and area  $A$  (see (1)–(2)) has the compactness

$$C = \frac{P^2}{4\pi A} < 0.8, \tag{4}$$

then it will be processed further because such a region consists of multiple connected objects and should be partitioned. A  $C$  of 0.8 turns out to be a suitable threshold for selecting only those objects in microscopic images of the central nervous system which need to be splitted.

### 2.6.2 Polygonal Approximation

A polygonal approximation is a transformation of a planar polygon into a polygon of less vertices. The digital boundary can be approximated with arbitrary accuracy by a polygon. The requirements are that the resulting polygon can be reconstructed by a few dominant points and that the principal structure of the contour should be conserved. During the last 30 years many heuristic algorithms have been considered for approximation of polygonal curves [51, 108]. About a dozen of different heuristic approaches to the problem can be accounted, and the number of algorithms exceeded one hundred items [52]. In some extent, the existence of a

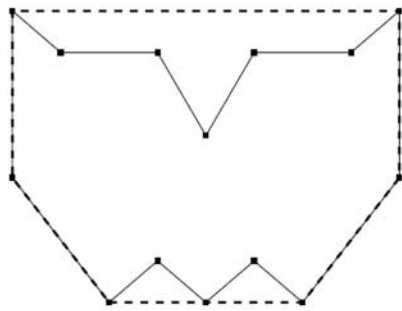


Fig. 3 Convex hull of the polygon

big amount and variety of the heuristic approximation algorithms can be explained by the variety of tasks, curve types, and error measures in use.

The most often applied approximation algorithm is a heuristic method called the Douglas-Peucker algorithm [28]. This iterative procedure repeatedly splits the curve into smaller and smaller curves until the maximum of the perpendicular distances of the points on the curve from the line segment is smaller than a certain error tolerance.

Here, we performed a quad tree decomposition of the contour followed by determining which contour points found by quad tree decomposition are lying inside, outside or on the contour [43]. To facilitate the detection of dominant points the contour is analyzed in terms of the Freeman-Chain-Code. We end up with a minimum-perimeter-polygon (MMP) presented by coordinates. The MMP presents the fewest vertices possible to capture the “essence” of the boundary shape. The list of points used for approximation of the polygon is  $L_{app}$ .

### 2.6.3 Concavities and Convexities of the MMP

Concavities and convexities are determined by evaluating  $L_{app}$ . For this the points  $P_i$  and  $P_{i+2}$  are connected. On the resulting line segment the midpoint  $T_i$  for each pair of points  $(P_i, P_{i+2})$  is determined.

$$T_i = \frac{1}{2}(P_i + P_{i+2}) \quad i = 0, \dots, n - 1 \quad \text{where we set}$$

$$P_n = P_0 \quad \text{and} \quad P_{n+1} = P_1.$$

If the midpoint lies on the contour line or within the polygon, then a convexity is given, otherwise a concavity. The resulting list of concavities  $L_{con}$  need to be classified to find corresponding points for the construction of split paths. On this the convex hull is constructed whereby vertices of the convex hull are connected with the corresponding point  $K$  of the concavities. Hence, we obtain the angle  $\alpha$  enclosed by the two line segments  $L_v$  and  $L_h$  (Fig. 4) whereby  $L_{max} = \max(|L_v|, |L_h|)$  between the vertices and the inclination point and the relative distance  $L_d = ||L_v| - |L_h||/L_{max}$  of

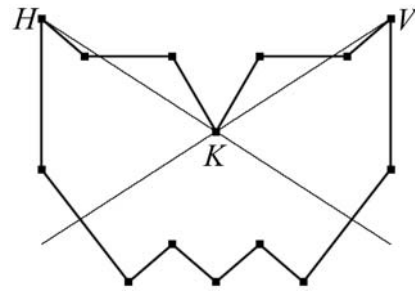


Fig. 4 Segment lines  $L_h$  and  $L_v$  passing  $K$

the line segments.  $L_d$  turns out to be a measure for the symmetry of the concavity with  $0 \leq L_d < 1$ . To evaluate these values the following thresholds were applied:

- angle thresholds  $\alpha_1$  and  $\alpha_2$  with  $0 < \alpha_1 < \alpha_2 < \pi$ .
- length thresholds  $L_1 > 0$  and  $L_2 > 0$ .
- relative difference threshold  $L_3 \in [0, 1]$ .

The order of a concavity is obtained after classification of the values by the thresholds:

- 1, if  $\alpha_2 < \alpha < \pi$ .
- 2, if  $\alpha_1 < \alpha \leq \alpha_2$  and  $L_{max} \leq L_1$  and  $L_d > L_3$ .
- 3, if  $\alpha_1 < \alpha \leq \alpha_2$  and  $L_{max} > L_1$  and  $L_d \leq L_3$ .
- 4, if  $\alpha \leq \alpha_1$  and  $L_{max} \leq L_2$ .
- 0, in all other cases.

As proposed by Wang [119] the following thresholds were used:  $\alpha_1 = \frac{\pi}{2}$ ,  $\alpha_2 = \frac{5}{6}\pi$ ,  $L_1 = L_2 = 20$  units of length (LE) and  $L_3 = 0.6$ .

### 2.6.4 Constructing Split Paths

Furthermore a *cost function* needs to be introduced to decide which *split paths* should be applied. As a starting point the vertex with the maximal concavity order is used. If there exist more than one maximum, the first maximum of  $L_{con}$  is considered. The line segments of a concavity can be elongated until they intersect with two other opposite parts of the polygon:

$$g_i : \vec{x} = \begin{pmatrix} V_{i,1} \\ V_{i,2} \end{pmatrix} + s \begin{pmatrix} K_{i,1} - V_{i,1} \\ K_{i,2} - V_{i,2} \end{pmatrix} \quad (\text{line segment } L_v)$$

$$h_i : \vec{x} = \begin{pmatrix} H_{i,1} \\ H_{i,2} \end{pmatrix} + t \begin{pmatrix} K_{i,1} - H_{i,1} \\ K_{i,2} - H_{i,2} \end{pmatrix} \quad (\text{line segment } L_h)$$

Here,  $g_i$  and  $h_i$  designate the equations of lines. For each concavity  $K_i$  there exist two points  $V_i$  and  $H_i$  which mark points of two vertices which pass opposite parts of the polygon. In between the resulting opposite intersection points we search for the corresponding opposite coordinate of the split path. The intersections of  $g_i$  and  $h_i$  with the polygon are calculated

$$e_j : \vec{x} = \begin{pmatrix} P_{j,1} \\ P_{j,2} \end{pmatrix} + u \begin{pmatrix} P_{j+1,1} - P_{j,1} \\ P_{j+1,2} - P_{j,2} \end{pmatrix} \quad \text{for } j = 0, \dots, n$$

and the whole boundary with  $j = 0, \dots, n$  is passed through. For each  $j$  we obtain the intersections by

$$(u, s) = (V_{i,1} - P_{j,1}, V_{i,2} - P_{j,2}) \times \begin{bmatrix} (P_{j,1} - P_{j,2}) & (P_{j+1,1} - P_{j+1,2}) \\ (K_{i,1} - V_{i,1}) & (K_{i,2} - V_{i,2}) \end{bmatrix}^{-1}$$

$$(u, t) = (H_{i,1} - P_{j,1}, H_{i,2} - P_{j,2}) \times \begin{bmatrix} (P_{j,1} - P_{j,2}) & (P_{j+1,1} - P_{j+1,2}) \\ (K_{i,1} - H_{i,1}) & (K_{i,2} - H_{i,2}) \end{bmatrix}^{-1}$$

If the intersection point lies in between  $P_j$  and  $P_{j+1}$  the opposite point for the split path is found. On this, the distance between the intersection points is determined:

$$d(P, Q) = |P - Q|.$$

The remaining concavities in the two regions  $A$  and  $B$  are those which are preserved after splitting and which are used for subsequent splittings. We set  $C = 0$  if the remaining concavities in  $A$  and  $B$  are uneven,  $C = 1$  if the number of concavities in  $A$  or  $B$  is even,  $C = 2$  if the number of concavities in  $A$  and  $B$  are even. The splitted regions have the areas  $A_A$  and  $A_B$ , see (2). The ratio of areas  $r_A(a)$  is the quotient of the minimum of  $A_A$  and  $A_B$  and the maximum of  $A_A$  and  $A_B$ :

$$r_A(a) = \frac{\min(A_A, A_B)}{\max(A_A, A_B)}.$$

Because it is not necessary to use for each class of concavities all parameters the following selections lead to robust classification results:

- $\text{deg}(S)$  = order of the starting point
- $\text{deg}(E)$  = order of the feasible end point
- $\text{opo}(S)$  = segment in between the intersections of  $L_v$  and  $L_h$  with the opposite part of the polygon that can be used for search of  $s$
- $\min(C)$  = minimum of  $C$
- $\min(d)$  = minimal distance of different feasible end points
- $\max(r)$  = maximal relative area of different feasible end points

### 2.7 Concavity Scale Space Approach

Using contour smoothing on a certain level scale regions can be analyzed independent of their size and their contour features like roughness or fractal dimension [21, 40, 61, 65, 87]. Furthermore, flat concavities that are important in the case of cell clump splitting are approximated by polygonal approximation to straight lines. Therefore, it turns out to be important to work on the original contours. However, small

concavities which contribute to the phenomenon of roughness should be smoothed.

First of all, we used the curvature (3) of the contour as introduced before for classifying concavities. Let  $D \subset Q$  be a simple connected  $C^2$ -domain. The boundary of  $D$  is a simple closed  $C^2$ -curve  $X : [a, b] \rightarrow Q$  with the parametrization  $X(t) = (x(t), y(t))$  whereby  $t \in [a, b]$ .

We need an approximate computation of the first and second derivatives of  $x(t)$  and  $y(t)$  for the determination of the curvature (3) of  $X$ . Here, we use symmetric difference quotients

$$x'(t) \approx \frac{1}{12h} (x(t - 2h) + 8x(t - h) - 8x(t + h) + x(t + 2h)), \tag{5}$$

$$x''(t) \approx \frac{1}{12h^2} (-x(t - 2h) + 16x(t - h) - 30x(t) + 16x(t + h) - x(t + 2h)) \tag{6}$$

with sufficiently small  $h > 0$ . Analogously, we approximate  $y'(t)$  and  $y''(t)$ .

Beside the calculation of curvature a suitable and invariant smoothing operation that works on a contour [16, 74] was realized by considering the contour in the complex plane [85]. Traveling anti-clockwise along this curve keeping constant speed, a complex function  $k(t)$  is obtained, where  $t$  can be considered as a time variable. The contour with the perimeter  $P$  is interpreted as a  $P$ -periodic function with regard to the arc length  $t$ :

$$k(t + P) = k(t) \quad (t \in \mathbb{R}).$$

The Euclidean plane  $\mathbb{R}^2$  can be considered as a complex plane  $\mathbb{C}$ :

$$k(t) = x(t) + iy(t) \quad (t \in \mathbb{R}).$$

If  $k$  is sufficient smooth, then the Fourier series of  $k$  converge uniformly to  $k$ .

$$k(t) = \sum_{k=-\infty}^{\infty} c_k \cdot e^{ik\omega t} \quad \left( \omega := \frac{2\pi}{P} \right)$$

Then it follows that  $k(t)$  can be approximated by a trigonometric polynomial of order  $N/2$  ( $N \gg 1$  even):

$$k(t) \approx \sum_{k=-N/2}^{(N/2)-1} c_k \cdot e^{ik\omega t}.$$

The coefficients  $c_k$  are denoted as Fourier coefficients. The vector of Fourier coefficients is the *Fourier descriptors* of the contour.

$$c_k = \frac{1}{P} \int_0^P k(t) \cdot e^{-ik\omega t} dt.$$

**Table 1** Survey of used parameters for the end point selection, resp. the opposite point of a concavity for split path generation

deg( $S$ )	4	4	4	3	3	3	2	2	1
deg( $E$ )	4-3	2-1	0	3	2-1	0	2	1	1
opo( $S$ )	use								
min( $C$ )	use	use		use	use		use	use	use
min( $d$ )	use	use			use		use	use	use
max( $r$ )	use		use			use			
$A \geq T_A$								use	use

To calculate the coefficients, the function  $k(t)$  is sampled at  $N$  points  $\frac{j}{N}P$  ( $j = 0, \dots, N - 1$ ). The outcome of this is the following representation:

$$k\left(\frac{j}{N}P\right) = \sum_{k=-N/2}^{(N/2)-1} \tilde{c}_k \cdot e^{ik\frac{2\pi}{P}\frac{j}{N}P} \quad (j = 0, \dots, N - 1).$$

The discrete Fourier transformation (DFT) for  $\tilde{c}_k$  is:

$$\begin{aligned} \tilde{c}_k &= \frac{1}{N} \sum_{j=0}^{N-1} k\left(\frac{j}{N}P\right) \cdot e^{-2\pi ikj/N} \\ &\approx c_k \left(k = -\frac{N}{2}, \dots, \frac{N}{2} - 1\right). \end{aligned}$$

If  $N$  is a power of 2, the fast Fourier transformation (FFT) can be applied.

In order to use for different images resp. objects comparable orders of smoothing the following normalization for the reconstruction of the contour by Fourier coefficients was used:

$$\text{scale} = \left\lfloor \frac{N \cdot G}{100} \right\rfloor. \tag{7}$$

Here, *scale* means the even number of Fourier coefficients that is used for the contour reconstruction,  $N$  is the number of contour coordinates and  $G$  is the order of smoothing. By using only a few coefficients of the descriptor the contour can be reconstructed and essential concavities filtered by the parameter *scale*. A reconstruction by increasing numbers of Fourier descriptors is shown in Fig. 5 and the scale space representation in Fig. 6.

### 2.7.1 Dominant Concavities and Cost Functions

Using a threshold for selecting a scale invariant smoothing we are able to filter dominant concavities which are relevant for planar shape partitioning. A subsequent step is the evaluation of feasible end points of a starting concavity. The evaluation is realized by comparing the possible areas  $A_A$  and  $A_B$  after splitting with a suitable threshold. If one area is smaller, the threshold of the related end point is removed

from the list of end points. If no end point remains in the list after evaluation, the splitting is terminated. Otherwise the relative length is calculated, whereby  $S$  is the starting point and  $E$  is the end point in between them and a solid line is constructed generating the two areas  $A$  and  $B$  with perimeters  $P_A$  and  $P_B$ . The relative length is the quotient of the distance between  $S$  and  $E$  and the minimum of  $P_A$  and  $P_B$  (*cost function 1*):

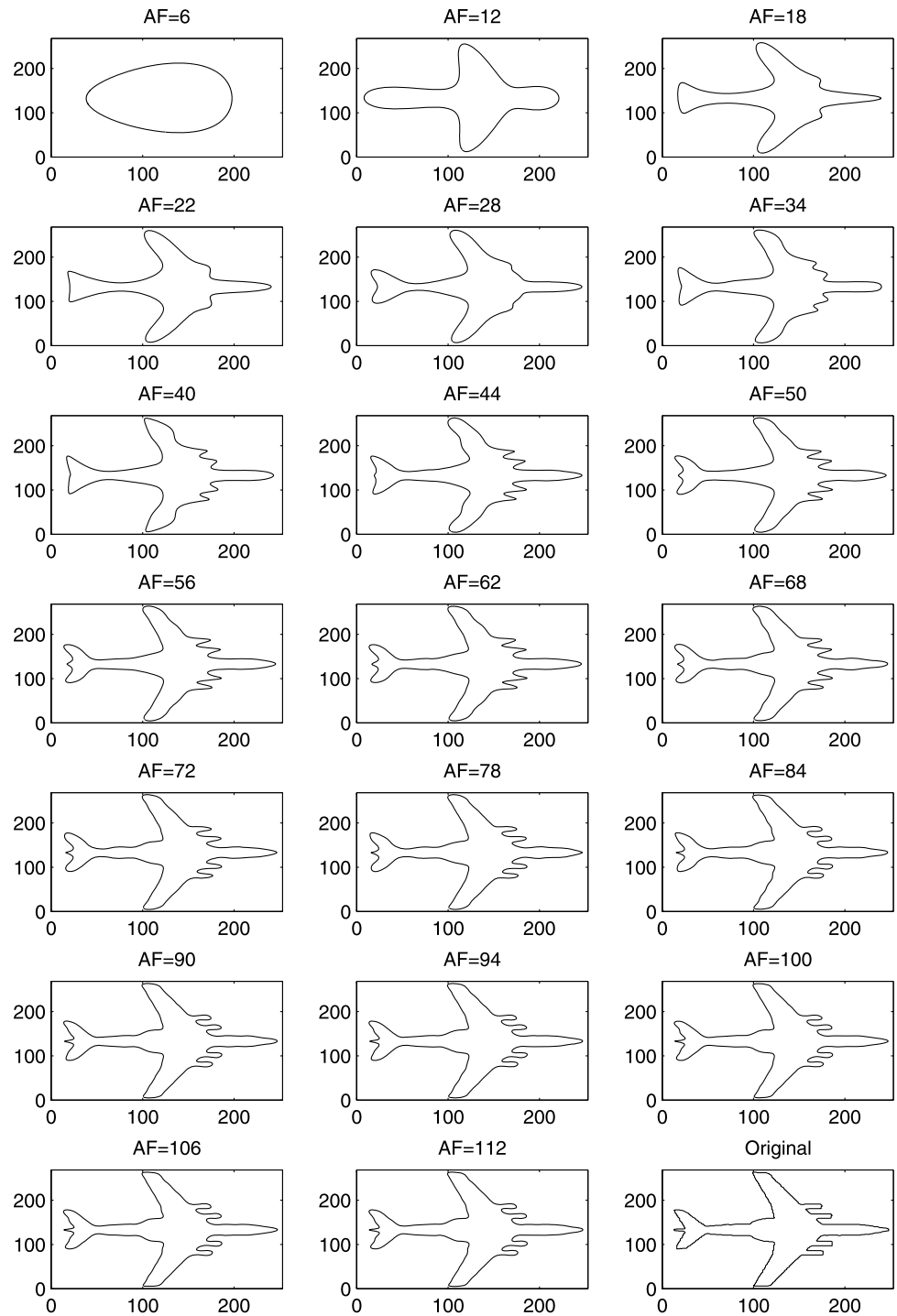
$$d_{rel}(E) = \frac{d(S, E)}{\min(P_A, P_B)}$$

A threshold of 0.35 guarantees that all regions have a perimeter larger than  $2|S - E| = 2d(S, E)$ . The *cost function 2* evaluates the lengths of  $S$  to all possible end points and a certain end point is selected which has the smallest distance to  $S$ . Furthermore, it is necessary to control if intersections of the splitting path with the curve occurs before the end point is reached. In such a case the end point with the next smallest distance is selected. If all end points do not fit the two cost functions, *cost function 3* is applied: The threshold for areas is tested and the maximum of curvature of the remaining points is determined whereby those points are selected where the curvatures are larger than 1/4 of the maximal curvature. The end point is calculated via the smallest distance of  $S$  to the opposite part of the curve and controlled for intersections with the curve before reaching the end point. If no end point can be determined the region is considered as non partitionable with respect to the criteria defined here and to perceptual grouping or biomorphological experience.

### 2.7.2 Double Connected Domains

Furthermore we must take double connected domains (domains with one hole) into account, since background areas enclosed by foreground may facilitate the partitioning of regions with large areas. Holes are determined by filling regions and subtracting images of filled regions from images without filled regions. If holes occur the connected regions are counted and administrated in a list  $L_{hole}$  of coordinates  $H_i$ . Holes are evaluated if they can be integrated into split paths. Hence, the length of the segment  $\overline{SE}$  with all

**Fig. 5** Smoothing by reducing the number of Fourier descriptors ( $AF =$  Number of Fourier descriptors)



contour points of a hole are determined. The same is done with  $E$  and the contour points of the hole. This is repeated with all holes. A hole is integrated into a split path if

$$d(S, H_i) + d(E, H_j) < \frac{d(S, E)}{2} \quad \text{for } i, j \in \{1, \dots, M\}$$

and  $H_i, H_j \in L_{hole}$

by minimizing the distances:

$$\min\{d(S, H_i) : H_i \in L_{hole} (i = 1, \dots, M)\}$$

$$\min\{d(E, H_j) : H_j \in L_{hole} (j = 1, \dots, M)\}$$

The coordinate list of the contour of the hole need to be partitioned according to the two new points  $H_i, H_j$  and combined with the second part of the region contour. Before this

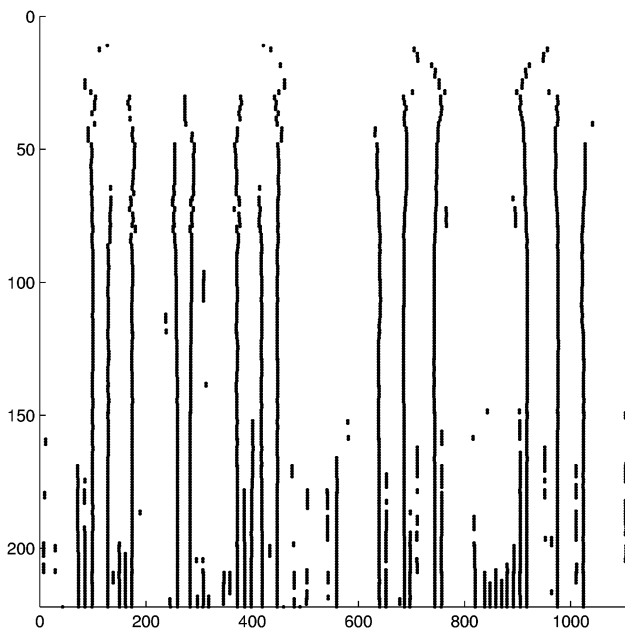


**Fig. 6** Concavity scale space representation of the example shown in Fig. 5. The *ordinate* presents the number of used Fourier coefficients for reconstructing the curve and the *abscissa* the index  $t$  of the curve. The points in the coordinate system are indicating the number of concavities at a certain scale, respectively, the number of Fourier coefficients used for reconstruction. Deep or strong concavities are represented by high stacks of points which can be reconstructed by a few Fourier coefficients

can be done it is necessary to determine the orientation of the coordinate lists and to adapt them all into the same direction (clockwise sorting). Finally, the original coordinate list of the integrated hole is removed. This method can be also applied to connected domains with several holes.

### 3 Results

In the following the results of the polygonal approximation based decomposition (PAD), the concavity scale space based decomposition (CSD) and the watershed based decomposition (WSD) in consideration of the expected decompositions (EXD) are presented.

#### 3.1 Watershed Based Decomposition (WSD)

There exist four principal preprocessing possibilities before the watershed algorithm is applied to an image:

- 1) binarization and calculating the distance transform,
- 2) smoothing the gray level image,
- 3) calculating the gradient image,
- 4) applying WSD to an image composed of inner and outer markers.

In order to facilitate the comparison gray level images were binarized followed by the distance and the watershed transformation.

The WSD leads to satisfying results if regions of an object do not exhibit too strong overlaps Fig. 7c, g, ä and Fig. 8c, f, i, l, o, r, u. However, even simple compositions of subregions like four overlapping objects Fig. 7k or small subregions positioned around a relative large area Fig. 7o, w can not be separated by the applied WSD. Furthermore, if the objects contain concave holes the WSD results are not optimal (Fig. 8o, r, u).

#### 3.2 Polygonal Approximation Based Decomposition (PAD)

The PAD was applied to images without holes. The decomposition domain of PAD are clearly objects that have many corners or discontinuities (Fig. 7e, m, q, u). Since objects contain deep and smooth concavities this method fails (Figs. 7i, 8a). Importantly, even if objects possess relative small corner-like concavities in regard to a large area of an object the PAD yields to acceptable results due to the concept of oppositeness of a concavity to be selected for a splitting path. This concept may lead to problems as shown in Fig. 7j where long split paths are preferred by the algorithm and not the cutting of relative small convexities of the object. At least it should be emphasized that the edge like appearance of the contours of the objects processed by the PAD which is visible especially in Fig. 7m, q and u derives from the approximation method.

#### 3.3 Concavity Scale Space Based Decomposition (CSD)

##### 3.3.1 Artificial Objects

The CSD approach turns out to subdivide objects possessing strong corners, continuous concavity mixtures and small convexities of their contours with respect to the area of the object. The parameters used by the CSD approach are the area, the curvature, the approximate distance, the radius for symmetric opening and the resizing factor for changes of the image size. A constant size of  $3 \times 3$  of the median filter as a preprocessing step turned out to be optimal with regard to the smoothness of the curve. The parameters used for partitioning the binary images in Figs. 7–10 are listed in Table 2.

Simple regions like Fig. 7b, f, j are partitioned as proposed by EXD. In Fig. 7n and v the subdivision shows the tendency of generating split paths to the opposite contour which yields to relative long split paths. Such long split paths are avoided in the EXD partitioned objects due to subdivide *harmonic* which means generating subregions of similar size and split paths meet at almost rectangular angles. If the objects are elongated like those in Figs. 7r and 8b, CSD leads to optimal results.

**Table 2** Parameters used for partitioning the images in Figs. 7–10 using the CSD approach. The first column *Image in Fig.* indicates the name of the subfigure. The parameters are described in Sect. 2.6.1

Image in Fig.	Area	Curvature	Distance	Resize	Opening
7b	50	0.3	1	1	3
7f	50	0.3	1	1	3
7j	200	0.1	1	1	3
7n	100	0.1	1	0.75	3
7r	65	0.1	2	0.5	3
7v	50	0.07	2	0.75	0
7z	65	0.07	2	0.5	0
8b	50	0.18	1	0.75	3
8e	65	0.07	2	0.5	0
8h	50	0.07	2	0.5	3
8k	65	0.07	2	0.5	3
8n	30	0.07	2	1	0
8q	30	0.07	2	1	0
8t	30	0.07	2	1	0
9b	50	0.1	2	0.5	3
9f	50	0.2	1	0.75	3
9j	8	0.1	1	0.25	3
9m	8	0.1	1	0.25	3
9p	35	0.1	1	2	2
9t	11	0.1	1	2	2
9x	11	0.15	1	2	3
10d	8	0.05	1	0.25	3
10f	18	0.15	1	0.4	3

The CSD algorithm is working robust on all changes of topology (Fig. 8e, h, k, n, q, t) of the object (Fig. 7z) with multiple continuous concavities. Starting with Fig. 7z the algorithm splits principal domains of convexity and performs internal splits of the object, too. The EXD result of this object shows a stronger orientation at the principal concavities and preventing at the same time a relative long split path separating the object in two large parts as presented in Fig. 7z. Introducing holes into the object yields to a stable incorporation of these topological background information. Figure 8e has obtained a rather similar partition as the EXD in Fig. 8g. Three overlapping holes (Fig. 8h) at the same position in the object as in Fig. 7e lead also to a similar result as shown in the proceeding Fig. 8e. If these holes are distributed within the object the splittings stay stable and are similar to those calculated in Fig. 8e and h. Splitting the object with a concave hole allows the generation of new split paths which are rather similar to the EXD result. Adding two new holes around the same concavity location as in Fig. 8n within the object Fig. 8q gives rise to a comparable result as in Fig. 8n. This means that the CSD approach can deal with complex topologies maintaining the principal pattern of split paths. If we go further and introduce an object into the concave hole

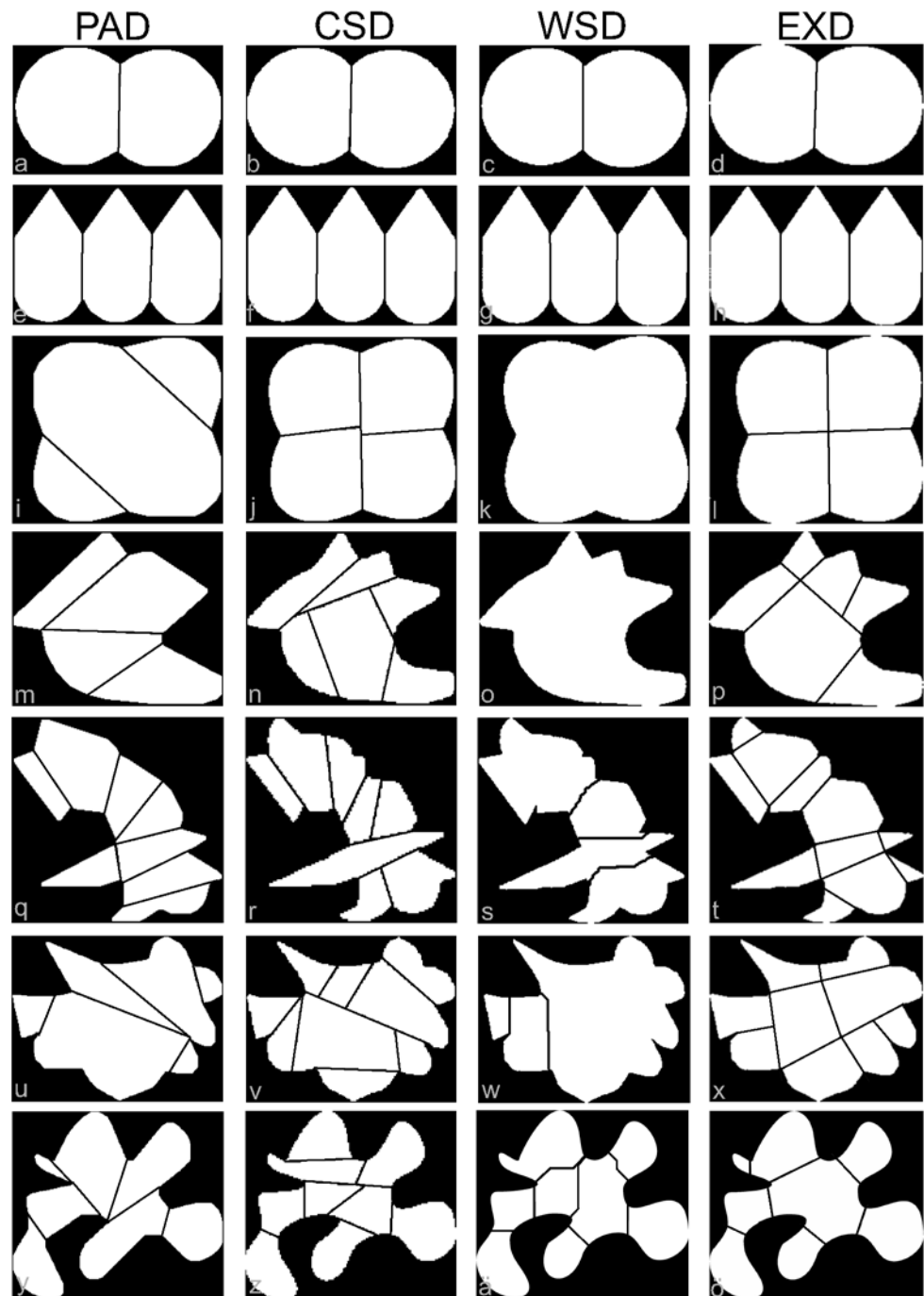
of the outer object Fig. 8t the CSD remains stable and split paths are still comparable as those found before on the same object with less topological complexity.

Applying CSD to the images of Liu and Srinath [62] (Fig. 9b, f) leads to satisfying partition results. However, small concavities are still connected to the larger mass of the object.

### 3.3.2 Video Microscopic and High Resolution Scan Cell Images

The images containing cells of the dentate gyrus (Fig. 9i, l) of a human brain were processed after segmentation. Several disjoint objects are covering the images which was directly transferred to the CSD algorithm meaning that the implementation can cope even with multiple non-connected objects. The objects are analyzed by the compactness parameter (4) in order to initialize a partitioning. Therefore, only objects covering stronger concavities of their contours are processed. Most of the cell areas as shown in the EXD images (Fig. 9k, n) are recovered. Three portions with strongly juxtaposed objects delimited by very low concavities are underpartitioned (Fig. 9j). The large cell cluster with a central hole in Fig. 9m shows an appropriate partitioning. The

**Fig. 7** Results of partitioning by polygonal approximation decomposition (PAD, in the *first column*), concavity scale space decomposition (CSD, *second column*), watershed decomposition (WSD, *third column*) and expected decomposition (EXD, *last column*). The latter was realized by an evaluator. Here, all objects are shown without holes. In (p), (t) and (x) are examples presented with mixtures of corners and continuous concavities. The WSD of (k), (o) and (w) do not lead to a partitioning of the objects



result of the CSD approach is presented in Fig. 10d and the expected objects in Fig. 10b. Comparing the CSD result of Fig. 10d to Fig. 10c of the WSD method shows obvious problems of the WSD technique at cell clusters with strong overlaps. Only those cell assemblies that do not overlap strongly are partitioned optimal. Small and few overpartitions can be seen also.

A cell cluster of the video microscopic image have been processed without surrounding objects and cell clusters (Fig. 10g) by the PAD and the CSD methods (Fig. 10e, f). As

in other examples the PAD algorithms show the tendency to generate very long split paths to opposite concavities of the contour. Furthermore, strong deviations with regard to the size and shape of disassembled objects are obvious. In contrast, the CSD approach has retrieved almost all expected components of this cell cluster.

The examples derived from high resolution transparent flat bed scanning of the mouse brain (Fig. 9o–z) show in the WSD (Fig. 9q, u, y) strong undersegmentations. Applying CSD the retrieval of those objects that were expected

**Fig. 8** Results of partitioning by polygonal approximation decomposition (PAD, in the *first column*), concavity scale space decomposition (CSD, *second column*), watershed decomposition (WSD, *third column*) and expected decomposition (EXD, *last column*). PAD is only applied to the object shown in the first row because the algorithm was realized for simple connected regions

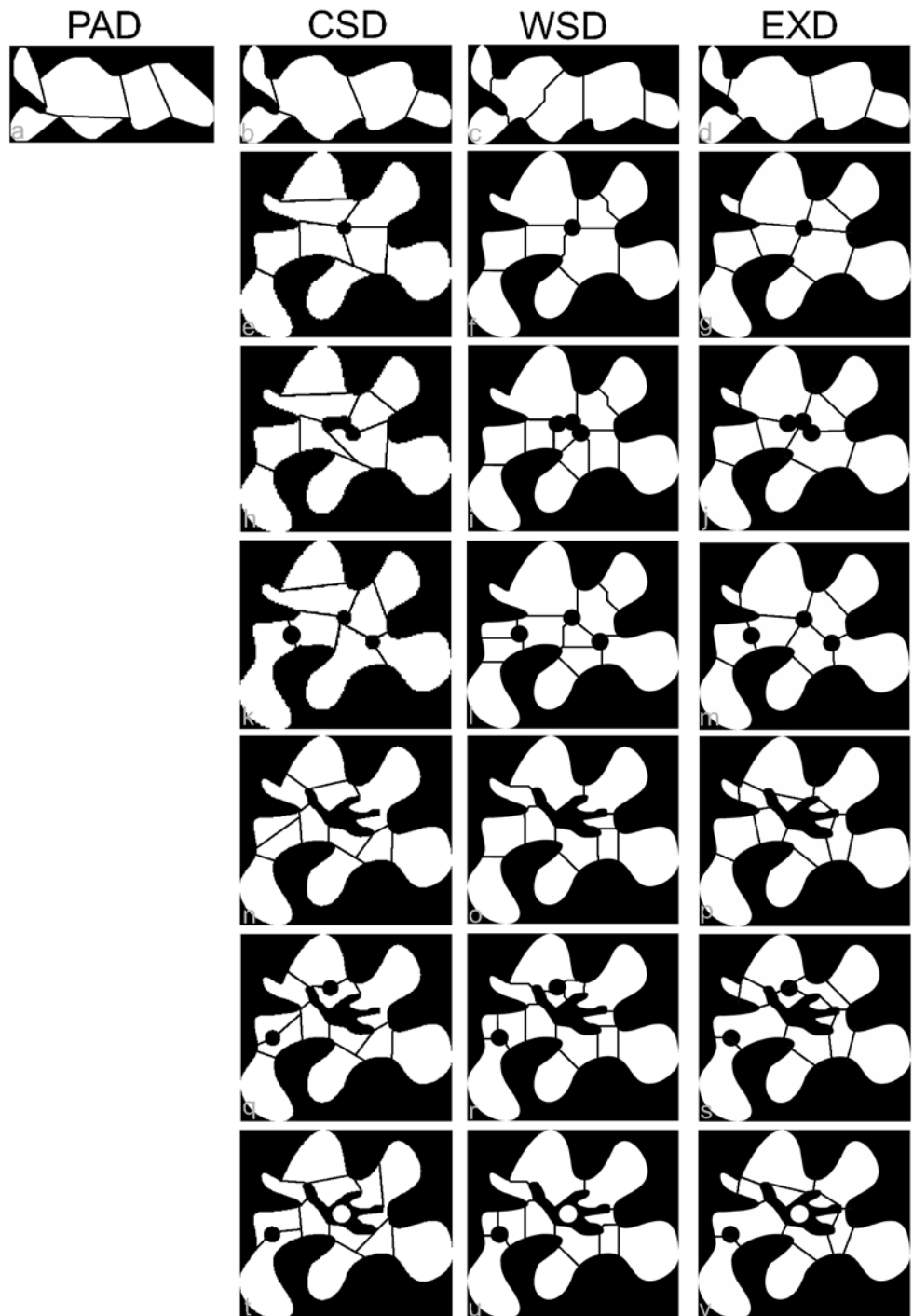


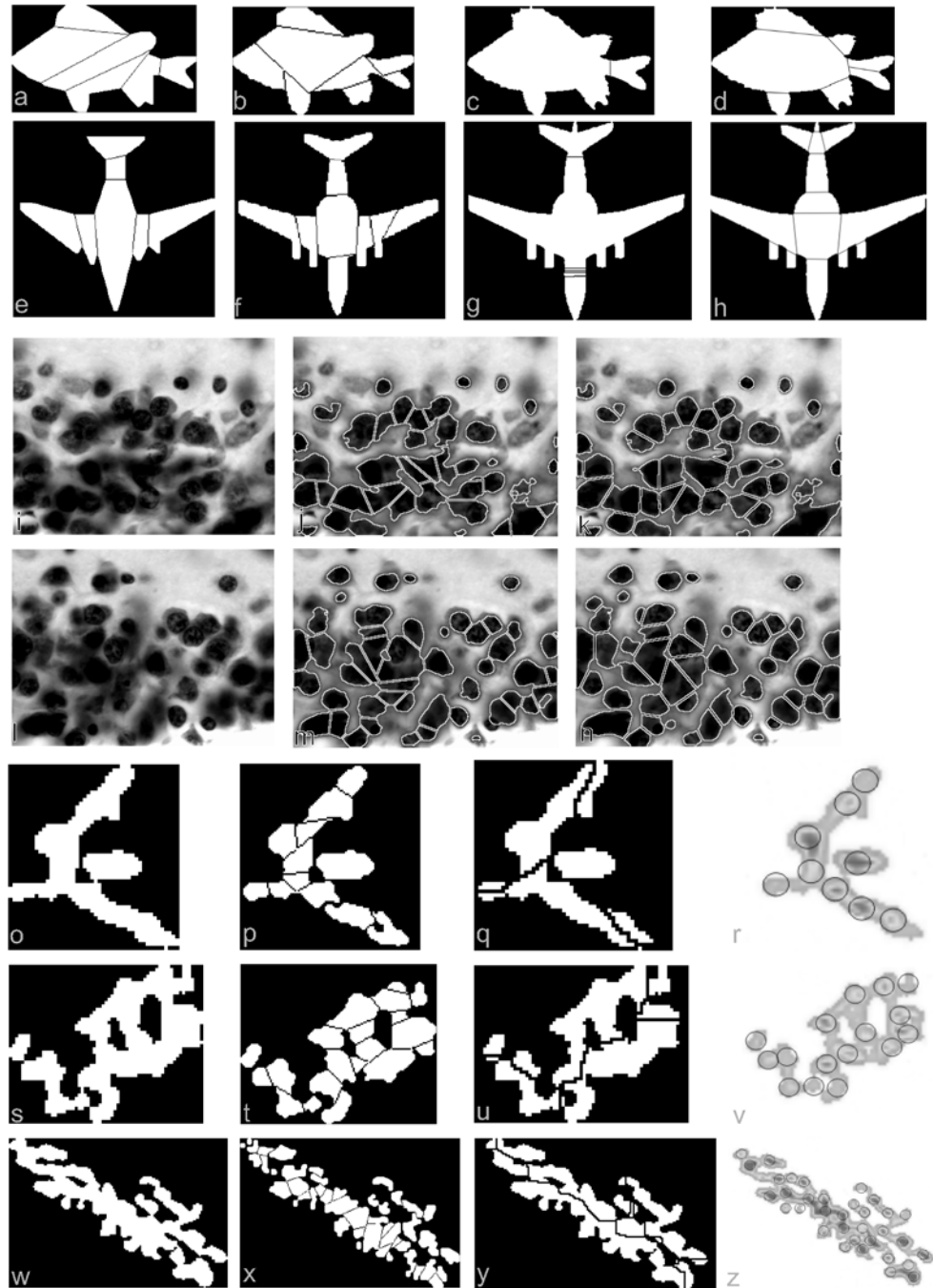
(Fig. 9r, v, z) yields to rather similar results. In Table 2 all parameters for the CSD approach that were applied to the images are presented. Images of the same category, for example, images derived from the high resolution transparent flat bed scanning of the mouse brain (Table 2: 7p, 7t, 7x) share the same range. The same holds true for the video microscopic images (Table 2: 7j, 7m). The artificial objects share the same range. However, according to the parameters

in Table 2 the images 5j and 5n have been segmented with rather large thresholds of the parameter area in comparison to the other objects.

### 3.3.3 Parametrization of CSD

The parameter space of the cell cluster in Fig. 10f have been explored. The parameters *area* and *curvature* are sensitive to the expected size and number of splitted objects. If the pa-

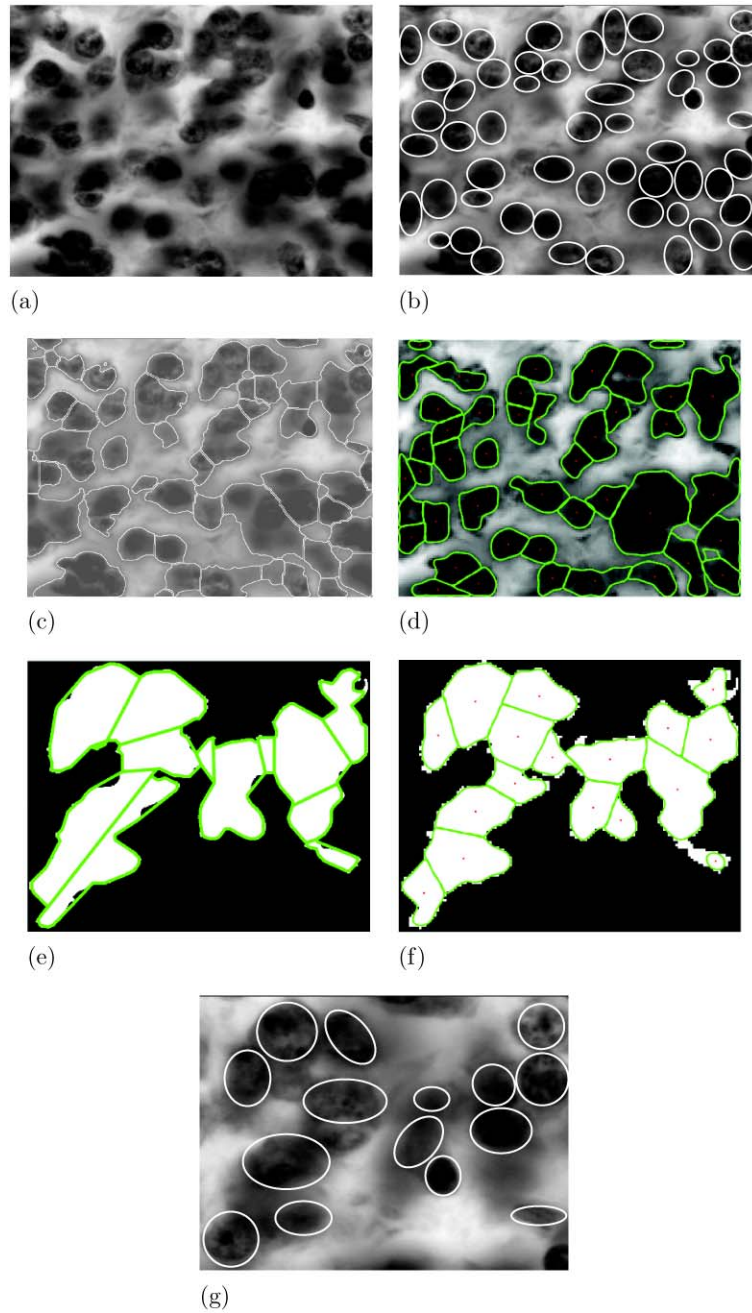
**Fig. 9** The first two rows (fish, airplane) are organized as follows: (a) PAD *first column*, (b) CSD *second column*, (c) WSD *third column* and (d) EXD *fourth column*. Subfigures (i) and (l) depict images captured by a video microscope and exhibiting cell clumps or optically fused neurons of the dentate gyrus. The binarized images were partitioned (j) and (m) by CSD with parameters as documented in Table 1. The EXD is shown in (k) and (n). Subfigures (o), (s) and (w) are showing binarized cell clusters derived from the high resolution flat bed scanned mouse brain. The EXD results are shown on gray level images (r), (v), (z) belonging to the CSD partitions (p), (t), (x). The corresponding WSD results are presented in (q), (u) and (y)



parameter *area* is small, e.g., in a range of 5–10 more objects will be splitted. If the curvature is small, e.g. in the range of 0.01–0.05 more objects will be splitted as well. Therefore, the parameter *area* should be determined in a pilot study, then the *curvature* have to be adapted to obtain appropriate split paths. The *size of the opening* operation is suitable to split elongated objects at the border periphery of a cell cluster. The size of the used symmetric structure element for the opening procedure must be chosen in dependence of expected object sizes. Cell clusters consist of almost el-

lipse shaped objects possessing more symmetry in contrast to the parts of the object in Fig. 9b. In this case the parameter should be set to 1. If the symmetries of the components are not too strong then this parameter should be 2. Therefore, parameters should be chosen in dependence of expected object sizes, structure of the cluster margin and the symmetry of singular objects. This means, only a few and efficient parameters are necessary to obtain an optimal splitting of cell clusters. Exploring the parameter space leads to a smooth increase of the number of objects and a smooth decrease of

**Fig. 10** EXD images contain circles or ellipses. **(a)** Video microscopic image. **(b)** EXD. **(c)** WSD. **(d)** CSD. A cell cluster from the upper right corner of **(a)** has been disassembled with PAD as shown in **(e)** and with CSD in **(f)**. Parameters cf. Table 2



the area and boundary of the splitted structure. Most important of the parameter exploration was the observation that no jumps in the number or size of splitted objects occur.

## 4 Discussion

### 4.1 Watershed and Polygonal Approximation Controlled Decomposition

The results of the two familiar approaches contour based decomposition (PAD) [13, 22, 23, 55, 56, 70, 89, 94, 102,

111, 115, 119, 124], and the watershed based decomposition (WSD) [11, 24, 57, 76, 117, 118] clearly exhibit more differences to the expected decompositions (EXD). We are aware of the problems concerning this way of evaluation because a quantitative comparison of segmentation results by using, e.g., the Hamming distance [37], the rank index, the global consistency error, the variation of information or the boundary error displacement would elevate the objectivity. These measures are suitable for benchmarking segmentation techniques, however, here we concentrate on splitting algorithms and differences to basic approaches like the watershed procedure.

The PAD can be applied successfully to object compositions with strong concavities or corners. Especially, shapes that are elongated or where objects are clustered in a chain-like manner can be partitioned efficiently by the PAD. The result of the PAD algorithm is strongly dependent on the granularity of the polygonal approximation. This depends on the size of the object as well as on the size of the image. The WSD is modified, optimized to the specific object segmentation problem and applied by most investigators [4, 11, 20, 24, 29, 57, 66, 76, 116–118]. Since the WSD can be accessed easily because it is implemented in many software packages for image analysis it became popular for many investigators. However, this approach has limitations in regard to cell clusters composed of cells with large differences of cell areas, shapes and center-to-center distances that are smaller than the radius of the assembled objects [57]. Here, we observed problems in terms of holes within clusters of objects. If juxtaposed objects share larger overlapping regions WSD becomes less effective. An obvious advantage of the WSD is the applicability to different kinds of pre-processed images. At least WSD can be easily adapted to multidimensional partition problems [58]. Since we aim to solve partitions of strongly clustered cells of different size and shape which may come up to huge and highly complex clusters the WSD is not suitable in terms of reliability.

#### 4.2 Scale Space Based Decomposition (CSD)

It turns out that the new approach, i.e., the concavity scale space based decomposition (CSD) offers some important advantages with regard to partitioning of objects covering features of

- convex and concave corners,
- convex and concave curves,
- geometric hierarchies of concavities and convexities, and
- domains with holes within clusters of objects.

An important feature of the CSD is its reliability with regard to similar split paths if holes are added to the same cluster of objects. It was shown that objects with strong concavities like the example of the binary airplane and the binary fish result in partitions that are rather similar like those derived from EXD. An disadvantage seems to be the adjustable space of parameters. However, in the case of cell clusters in biological tissues repeating patterns of object compositions appear which restricts the space of parameters considerable. A nonparametric version or self adjusting version of the current CSD could be acquired by (1) developing a new contour or shape analysis and (2) considering further formalizable heuristics of cognitive-psychologic analysis of partitioning object shapes [25, 99, 105, 107]. So far, a 3D extension of the CSD is not available whereby the WSD technique can be adapted easily to 3D splitting problems. The generation of

split paths within a certain scale results in slight dislocation with regard to details of regions after applying them directly to the original object cluster. However, such dislocations are small and do not lead to wrong locations of partitioned objects within an object cluster. Therefore, this phenomenon can be disregarded. It is now clear that, in addition to strong overlaps of regions holes within regions can be integrated into split paths. This observation suggests, that compared to other studies the CSD approach has some principal advantages concerning partitioning of clustered regions with emerging complexity. At this point of time, however, it has not been possible to identify clearly separate cells in huge clusters of several thousands of cells each composed of a few pixels which are derived from high resolution flat bed scanning. Therefore, this issue is considered currently by developing pre-partitioning steps and paralleled algorithms. We believe that the CSD approach, while not definitive, will provide a useful framework for future investigation of strategies of decomposing highly complex aggregations of biological cells.

**Acknowledgements** The authors gratefully acknowledge the encouragement and valuable criticism of Prof. Manfred Tasche of the Institute of Mathematics and Prof. Andreas Wree of the Institute of Anatomy of the University of Rostock.

#### References

1. Abe, K.: Parts of planar shapes. *Pattern Recogn.* **29**, 1703–1711 (1996)
2. Adiga, P., Chaudhuri, B., Rodenacker, K.: Semi-automatic segmentation of tissue cells from confocal microscope images. In: *ICPR'96*, pp. 494–497 (1996)
3. Agam, G., Dinstein, I.: Geometric separation of partially overlapping nonrigid objects applied to automatic chromosome classification. *IEEE Trans. Pattern Anal. Mach. Intell.* **19**, 1212–1222 (1997)
4. Ancin, H., Dufresne, T.E., Ridder, G.M., Turner, J.N., Roysam, B.: An improved watershed algorithm for counting objects in noisy, anisotropic 3-d biological images. In: *ICIP '95: Proceedings of the 1995 International Conference on Image Processing*, vol. 3, p. 3172. *IEEE Comput. Soc.*, Washington (1995)
5. Ancin, H., Roysam, B., Dufresne, T., Chestnut, M., Ridder, G., Szarowski, D., Turner, J.: Advances in automated 3-d image analyses of cell populations imaged by confocal microscopy. *Cytometry* **25**, 221–234 (1996)
6. Anoraganingrum, D.: Cell segmentation with median filter and mathematical morphology operation. In: *Proc. 10th International Conference on Image Analysis and Processing*, vol. 10, pp. 1043–1046 (1999)
7. Attneave, F.: Some informational aspects of visual perception. *Psychol. Rev.* **61**, 183–193 (1954)
8. Bamford, P., Jackway, P., Lovell, B.: Progress in the robust automated segmentation of real cell images. *SPIE* **3747**, 34–56 (1999)
9. Barenholtz, E., Cohen, E., Feldman, J., Singh, M.: Detection of change in shape: an advantage for concavities. *Cognition* **89**, 1–9 (2003)

10. Bengtsson, E.: Computerized cell image analysis: past present, and future. In: LNCS, vol. 2749, pp. 395–407 (2003)
11. Bengtsson, E., Wählby, C., Lindblad, J.: Robust cell image segmentation methods. *Pattern Recogn. Image Anal.* **14**, 157–167 (2004)
12. Bertamini, M., Croucher, C.: The shape of holes. *Cognition* **87**, 33–54 (2003)
13. Bilodeau, G.-A.: Part segmentation of objects in real images. *Pattern Recogn.* **35**, 2913–2926 (2002)
14. Blum, H.: A Transformation for Extracting New Descriptions of Shape, p. 362 (1967)
15. Braquelaire, J., Brun, L.: Image segmentation with topological maps and interpixel representation. *J. Vis. Commun. Image Represent.* **9**, 62–79 (1998)
16. Cao, F.: Geometric curve evolution and image processing. In: LNM, vol. 1805, pp. 1–187 (2003)
17. Chen, X., Yu, C.: Application of some valid methods in cell segmentation. In: SPIE, vol. 4550, pp. 340–344 (2001)
18. Clocksin, W.: Automatic segmentation of overlapping nuclei with high background variation using robust estimation and flexible contour models. In: ICIAP, vol. 1, pp. 682–687 (2003)
19. Cornsweet, T.: *Visual Perception*. Academic Press, New York (1970)
20. Costa, J., Mascarenhas, D., Marcio, L., de Andrade Netto, M.: Cell nuclei segmentation in noisy images using morphological watersheds. In: SPIE, vol. 3164, pp. 314–324 (1997)
21. Costa, L., Cesar, R.M.: *Shape Analysis and Classification: Theory and Praxis*. CRC Press, Boca Raton (2001).
22. Cronin, T.: A boundary concavity code to support dominant point detection. *Pattern Recogn. Lett.* **20**, 617–634 (1999)
23. Cronin, T.: Visualizing concave and convex partitioning of 2d contours. *Pattern Recogn. Lett.* **24**, 429–443 (2003)
24. Cui, Y., Zhou, N.: Blob analysis using watershed transformation. In: LNAI, vol. 1821, pp. 482–491 (2000)
25. de Winter, J., Wagemans, J.: Segmentation of object outlines into parts: a large-scale integrative study. *Cognition* **99**, 275–325 (2006)
26. Dejnozkova, E., Dokladal, P.: Modelling of overlapping circular objects based on level set approach. In: LNCS, vol. 3211, pp. 416–423 (2004)
27. Dias, A.V., Pianço-Diniz, C., Garçon, S.: Segmentation of neurons using mathematical morphology. In: IAPR, vol. 1, pp. 435–438 (1998)
28. Douglas, D., Peucker, T.: Algorithm for the reduction of the number of points required to represent a line or its caricature. *Can. Cartogr.* **10**, 112–122 (1973)
29. Dow, A., Shafer, S., Waggoner, A.: Morphological segmentation of multi-probe fluorescence images for immunophenotyping in melanoma tissue sections. In: SPIE, vol. 2055, pp. 487–498 (1993)
30. Du, H., Qin, H.: Medial axis extraction and shape manipulation of solid objects using parabolic PDEs. In: SM '04: Proceedings of the ninth ACM symposium on Solid modeling and applications, pp. 25–35 (2004)
31. Eschenbach, C., Habel, C., Kulik, L., Leßmöllmann, A.: Shape nouns and shape concepts: a geometry for 'corner'. In: LNCS, vol. 1404, pp. 177–203 (1998)
32. Fantoni, C., Gerbino, W.: Contour interpolation by vector-field combination. *J. Vis.* **3**, 281–303 (2003)
33. Feldman, J., Singh, M.: Information along contours and objects. *Psychol. Rev.* **112**, 243–252 (2005)
34. Feng, H.-Y., Pavlidis, T.: Decomposition of polygons into simpler components: feature generation for syntactic pattern recognition. *IEEE Trans. Comput.* **24**, 636–650 (1975)
35. Fischler, M., Wolf, H.: Locating perceptually salient points on planar curves. *IEEE Trans. Pattern Anal. Mach. Intell.* **16**, 113–129 (1994)
36. Foran, D., Berg, R.: A method for quantitative image assessment based on redundant feature measurements and statistical reasoning. *Comput. Methods Programs Biomed.* **45**, 291–305 (1994)
37. Freixenet, J., Muñoz, X., Raba, D., Martí, J., Cufí, X.: Yet another survey on image segmentation: Region and boundary information integration. In: LNCS, vol. 2352, p. 408422 (2002)
38. Gallyas, F., Hsu, M., Buzsaki, G.: Four modified silver methods for thick sections of formaldehyde-fixed mammalian central nervous tissue: 'dark' neurons, perikarya of all neurons, microglial cells and capillaries. *J. Neurosci. Methods* **50**, 159–164 (1993)
39. Garrido, A., de la Blanca, N.P., Garcia-Silvente, M.: Cell image segmentation. In: SCIA, vol. 1, pp. 659–665 (1997)
40. Gauch, J.: *Multiresolution Image Shape Description*. Springer, New York (1992)
41. Geusebroek, J.M., Smeulders, A.W.M., Cornelissen, F.: Segmentation of cell clusters by nearest neighbour graphs. In: ASCI'97, Proceedings of the third annual conference of the Advanced School for Computing and Imaging, pp. 248–252 (1997)
42. Geusebroek, J.M., Smeulders, A.W.M., Cornelissen, F., Geerts, H.: Segmentation of tissue architecture by distance graph matching. *Cytometry* **35**(1), 12–22 (1999)
43. Gonzalez, R., Woods, R., Eddins, S.: *Digital Image Processing Using Matlab*. Prentice Hall, Upper Saddle River (2004)
44. Gose, E.E., Rose, W.H., Barnes, W.E., Kaplan, E., Arnold, J.S.: Decomposition of image sequences of overlapping homogeneous transparent radiating objects. In: A Comparison of Some Segmentation Algorithms for Cytology, pp. 971–973 (1980)
45. Grinaker, S.: Edge based segmentation and texture separation. In: A Comparison of Some Segmentation Algorithms for Cytology, pp. 554–557 (1980)
46. Haralick, R., Shapiro, L.: Image segmentation techniques. *Comput. Vis. Graph. Image Process.* **29**, 100–132 (1985)
47. Held, A., Abe, K.: On the decomposition of binary shapes into meaningful parts. *Pattern Recogn.* **27**, 637–647 (1994)
48. Hoffman, D., Singh, M.: Saliency of visual parts. *Cognition* **63**, 29–78 (1997)
49. Jayasooriah, S., Yeow, H., Sinniah, R.: Decomposition of digital clumps into convex parts by contour tracing and labelling. *Pattern Recogn. Lett.* **13**, 789–795 (1992)
50. Kailay, B., Sadananda, R., Das, J.: An algorithm for segmenting juxtaposed objects. *Pattern Recogn.* **13**, 347–351 (1981)
51. Kim, C., Sklansky, J.: Digital and cellular convexity. *Pattern Recogn.* **15**, 359–367 (1982)
52. Kolesnikov, A.: Efficient algorithms for vectorization and polygonal approximation. Ph.D. thesis, University of Joensuu, Joensuu, Finland (2003)
53. Lam, R., Ip, H., Li, C.: Approaches to decompose flat structuring element for fast overlapping search morphological algorithm. In: ICPR, vol. 2, pp. 1461–1463 (1998)
54. Leavers, V.: *Shape Detection in Computer Vision Using the Hough Transform*. Springer, Berlin (1992)
55. Lee, T., Atkins, M.: A new approach to measure border irregularity for melanocytic lesions. In: SPIE, vol. 3979, pp. 668–675 (2000).
56. Lee, T., Atkins, M., Li, Z.-N.: Indentation and protrusion detection and its applications. In: LNCS, vol. 2106, pp. 335–343 (2001)
57. Lee, Y.-K., Kim, J.-H.: An efficient morphological segmentation for significantly overlapped particles. In: SPIE, vol. 2424, pp. 349–357 (1995)
58. Lin, G., Adiga, U., Olson, K., Guzowski, J., Barnes, C., Roysam, B.: A hybrid 3d watershed algorithm incorporating gradient cues and object models for automatic segmentation of nuclei in confocal image stacks. *Cytometry* **56**, 23–36 (2003).
59. Lin, G., Chawia, M., Olson, K., Guzowski, J., Barnes, C., Roysam, B.: Hierarchical, model-based merging of multiple fragments for improved three-dimensional segmentation of nuclei. *Cytometry* **63**, 20–33 (2004)

60. Lindblad, J., Wählby, C., Bengtsson, E., Zaltsman, A.: Image analysis for automatic segmentation of cytoplasm and classification of rac1 activation. *Cytometry* **57**, 22–33 (2004)
61. Lisani, J., Moisan, L., Monasse, P., Morel, J.: On the theory of planar shape. *Multiscale Model. Simul.* **1**, 1–24 (2003)
62. Liu, H.-C., Srinath, M.: Corner detection from chain-code. *Pattern Recogn.* **21**, 51–68 (1990)
63. Liu, L., Sclaroff, S.: Region segmentation via deformable model-guided split and merge. In: *ICCV*, vol. 1, pp. 98–104 (2001)
64. Liu, Z., Jacobs, D., Basri, R.: The role of convexity in perceptual completion: beyond good continuation. *Vis. Res.* **39**, 4244–4257 (1999)
65. Loncaric, S.: A survey of shape analysis techniques. *Pattern Recogn.* **31**, 983–1001 (1998)
66. Loukas, C., Wilson, G., Vojnovic, B.: Automated segmentation of cancer cell nuclei in complex tissue sections. In: *SPIE*, vol. 4158, pp. 188–198 (2001)
67. Lowe, D.: *Perceptual Organization and Visual Recognition*. Kluwer Academic, New York (1985)
68. Malladi, R.: *Geometric Methods in Bio-Medical Image Processing*. Springer, Berlin (2001)
69. Malpica, N., de Solorzano, C.O., Vaquero, J., Santos, A., Vallcorba, I., Garcia-Sagredo, J.M., del Pozo, F.: Applying watershed algorithms to the segmentation of clustered nuclei. *Cytometry* **28**, 289–297 (1997)
70. Marji, M., Siy, P.: Polygonal representation of digital planar curves through dominant point detection—nonparametric algorithm. *Pattern Recogn.* **37**, 2113–2130 (2004)
71. Metzler, V., Lehmann, T., Aach, T.: Morphological multiscale shape analysis of light micrographs. In: *SPIE*, vol. 3961, pp. 227–238 (2000)
72. Modersitzki, J.: *Numerical Methods for Image Registration*. Oxford University Press, London (2004)
73. Mokhtarian, F., Bober, M.: Curvature Scale Space Representation: Theory, Applications, and MPEG-7 Standardization. *Computational Imaging and Vision*, vol. 25. Springer, Berlin (2003)
74. Mokhtarian, F., Mackworth, A.: A theory of multi-scale, curvature-based shape representation for planar curves. *IEEE Trans. Pattern Anal. Mach. Intell.* **14**, 789–805 (1992)
75. Nedzved, A., Ablameyko, S., Pitas, I.: Morphological segmentation of histology cell images. In: *15th International Conference on Pattern Recognition (ICPR'00)*, vol. 1, pp. 1500–1504 (2000)
76. Nilsson, B., Heyden, A.: Segmentation of dense leukocyte clusters. In: *Proc. MMBIA*, vol. 1, pp. 221–227 (2001)
77. Norman, J., Phillips, F., Ross, H.: Information concentration along the boundary contours of naturally shaped solid objects. *Perception* **30**, 1285–1294 (2001)
78. Ong, S.: Image analysis of tissue sections. *Comput. Biol. Med.* **26**, 269–279 (1996)
79. Otsu, N.: A threshold selection method from gray level histograms. *IEEE Trans. Syst. Man. Cybern.* **9**, 62–66 (1979)
80. Pal, N., Pal, S.: A review on image segmentation techniques. *Pattern Recogn.* **26**, 1277–1294 (1993)
81. Pavlidis, T., Horowitz, S.: Segmentation of plane curves. *IEEE Trans. Comput.* **23**, 860–870 (1974)
82. Pieroni, G.G., Costabile, M.F., Guerra, G.: Decomposition of shape boundaries in a problem of map sequence analysis. In: *A Comparison of Some Segmentation Algorithms for Cytology*, pp. 618–623 (1980)
83. Pinker, S.: Visual cognition: An introduction. *Cognition* **18**, 1–63 (1984)
84. Pizer, S., Fritsch, D., Yushkevich, P., Johnson, V., Chaney, E.: Segmentation, registration, and measurement of shape variation via image object shape. *IEEE Trans. Med. Imaging.* **18**, 851–865 (1999)
85. Reiss, T.: *Recognizing Planar Objects Using Invariant Image Features*. Springer, New York (1993)
86. Resnikoff, H.: *The Illusion of Reality: Topics in Information Science*. Springer, New York (1985)
87. Rodenacker, K., Bengtsson, E.: A feature set for cytometry on digitized microscopic images. *Anal. Cell. Pathol.* **25**, 1–36 (2003)
88. Roerdink, J., Meijster, A.: The watershed transform: Definitions, algorithms and parallelization strategies. *Fundam. Inform.* **41**, 187–228 (2001)
89. Rosin, P.: Shape partitioning by convexity. *IEEE Trans. Syst. Man. Cybern. Part A* **30**, 202–210 (2000)
90. Rougon, N., Prêteux, F.: Directional adaptive deformable models for segmentation. *J. Electron. Imag.* **7**, 231–256 (1998)
91. Rowinski, J., Souchier, C., Czyba, J., Pages, M., Fages, R., Laurent, J., Greenland, T.: Morphometric studies of cell nuclei by means of image analysis and computer data processing. *Gegenbaurs Morphol. Jahrb.* **126**, 253–263 (1980)
92. Rutkowski, W.: Shape segmentation using arc-chord properties. *Comput. Graph. Image Process.* **17**, 114–129 (1981)
93. Sahoo, P., Soltani, S., Wong, A., Chen, Y.: A survey of thresholding techniques. *Comput. Vis. Graph. Image Process.* **41**, 233–260 (1988)
94. Salotti, M.: An efficient algorithm for the optimal polygonal approximation of digitized curves. *Pattern Recogn. Lett.* **22**, 215–221 (2001)
95. Schmitt, O., Eggers, R.: Systematic investigations of the contrast results of histochemical stainings of neurons and glial cells in the human brain by means of image analysis. *Micron* **28**, 197–215 (1997)
96. Schmitt, O., Eggers, R.: Flat-bed scanning as a tool for quantitative neuroimaging. *J. Microsc.* **196**, 337–346 (1999)
97. Schmitt, O., Eggers, R., Modersitzki, J.: Videomicroscopy, image processing, and analysis of whole histologic sections of the human brain. *Microsc. Res. Tech.* **66**, 203–218 (2005)
98. Schüpp, S., Elmoataz, A., Fadili, M.-J., Bloyet, D.: Fast statistical level sets image segmentation for biomedical applications. In: *LNCS*, vol. 2106, pp. 380–388 (2001)
99. Schwartz, N.: Estimating curvature of nondifferentiable functions and complex shape contours. *Percept. Mot. Ski.* **101**, 362–364 (2005)
100. Sclaroff, S., Liu, L.: Deformable shape detection and description via model-based region grouping. *IEEE Trans. Pattern Mach. Intell.* **23**, 475–489 (2001)
101. Serpico, S., Vernazza, G., Dellepiane, S.: Merging of different segmentation techniques for sell image recognition. In: *SPIE*, vol. 1027, pp. 208–213 (1988)
102. Shah, J.: Segmentation of shapes. In: *LNCS*, vol. 2106, pp. 236–244 (2001)
103. Shannon, C.: A mathematical theory of communication. *Bell Syst. Techn. J.* **27**, 379–423 (1948)
104. Sheu, H., Hu, W.-C.: Multiprimitive segmentation of planar curves—a two-level breakpoint classification and tuning approach. *IEEE Pattern Anal. Mach. Intell.* **21**, 791–797 (1999)
105. Siddiqi, K., Kimia, B.: Parts of visual form: computational aspects. *IEEE Trans. Pattern Anal. Mach. Intell.* **17**, 239–251 (1995)
106. Siddiqi, K., Tresness, K., Kimia, B.: Parts of visual form: psychophysical aspects. *Perception* **25**, 399–424 (1996)
107. Singh, M., Seyranian, G., Hoffman, D.: Parsing silhouettes: The short-cut rule. *Percept. Psychophys.* **61**, 636–660 (1999)
108. Sklansky, J., Chazin, R., Hansen, B.: Minimum perimeter polygons of digitized silhouettes. *IEEE Trans. Comput.* **21**, 260–268 (1972)
109. Stephansson, O., Wang, W., Dahlhielm, S.: Automatic image processing of aggregates. In: *ISRM Symposium: Eurock'92*, pp. 31–35 (1992)

110. Szegin, M., Sankur, B.: Survey over image thresholding techniques and quantitative performance evaluation. *J. Electron Imag.* **13**, 146–165 (2004)
111. Talbot, H., Appleton, B.: Elliptical distance transforms and the object splitting problem. In: *Proceedings of ISMM2002*, pp. 229–240 (2002)
112. Thompson, D., Bartels, H., Haddad, J., Bartels, P.: Scene segmentation in a machine vision system for histopathology. In: *SPIE*, vol. 1206, pp. 40–47 (1990)
113. Thórisson, K.: Simulated perceptual grouping: An application to human-computer interaction. In: *Proceedings of the 16th Annual Conference of Cognitive Science Society*, Atlanta, GA, pp. 876–881 (1994)
114. Todman, A., Claridge, E.: Low-level grouping mechanisms for contour completion. *Inf. Sci.* **125**, 19–35 (2000)
115. Tănase, M., Veltkamp, R.: Polygon decomposition based on the straight line skeleton. In: *SoCG*, vol. 1, pp. 58–67 (2003)
116. van Ham, P., de Hauwer, C., Kiss, R.: Dynamic behaviour analysis of in vitro cancerous cells by means of an automatic image processing device. In: *SPIE*, vol. 2710, pp. 967–978 (1996)
117. Wählby, C., Bengtsson, E.: Segmentation of cell nuclei in tissue by combining seeded watersheds with gradient information. In: *LNCS*, vol. 2749, pp. 408–414 (2003)
118. Wählby, C., Sintorn, I.-M., Erlandsson, F., Borgefors, G., Bengtsson, E.: Combining intensity, edge and shape information for 2d and 3d segmentation of cell nuclei in tissue sections. *J. Microsc.* **215**, 67–76 (2004).
119. Wang, W.: Binary image segmentation of aggregates based on polygonal approximation and classification of concavities. *Pattern Recogn.* **31**, 1503–1524 (1998)
120. Weszka, J.: A survey of threshold selection techniques. In: *CGIP*, vol. 7, pp. 259–265 (1978)
121. Wu, H.-S., Barba, J., Gil, J.: A parametric fitting algorithm for segmentation of cell images. *IEEE Trans. Biomed. Eng.* **45**, 400–407 (1998)
122. Xu, J.: Morphological decomposition of 2-d binary shapes into conditionally maximal convex polygons. *Pattern Recogn.* **29**, 1075–1104 (1996)
123. Yang, F., Jiang, T.: Cell image segmentation with kernel-based dynamic clustering and an ellipsoidal cell shape model. *J. Biomed. Inf.* **34**, 67–73 (2001)
124. Yang, Q., Parvin, B.: Harmonic cut and regularized centroid transform for localization of subcellular structures. *IEEE Trans. Biomed. Eng.* **50**, 469–475 (2003)
125. Yeo, T., Jin, X., Ong, S., Jayasooriah, S., Sinniah, R.: Clump splitting through concavity analysis. *Pattern Recogn. Lett.* **15**, 1013–1018 (1994)
126. Zhang, D., Lu, G.: Review of shape representation and description techniques. *Pattern Recogn.* **37**, 1–19 (2004)
127. Zhang, Y.: Evaluation and comparison of different segmentation algorithms. *Pattern Recogn. Lett.* **18**, 963–974 (1997)
128. Zusne, L.: *Visual Perception and Form*. Academic Press, San Diego (1970)



**Oliver Schmitt** received his M.D. degree in Medicine 1991 and his Ph.D. degree 1993 from the University of Lübeck in Germany. He is currently Associate Professor of Anatomy at the University of Rostock. His technical interests are distributed image processing, image registration, image segmentation, computer vision, high resolution small animal brain MRI, virtual slide analysis and pattern classification.



**Stephan Reetz** received his M.S. degree in Mathematics in 2007 from the University of Rostock in Germany. He is currently system administrator and junior lecturer in mathematics and informatics at the Academy of Technology. His technical interests are image segmentation, medical imaging, computer vision and video processing.